

Received August 28, 2018; reviewed; accepted November 21, 2018

Novel (Ag,Y) doped TiO₂ plasmonic photocatalyst with enhanced photocatalytic activity under visible light

Wannes Kallel, Sirine Chaabene, Soraa Bouattour

University of Sfax-Faculty of Science-Laboratory CI, Sfax, Tunisia

Corresponding author: wanneskallel@yahoo.fr (Wannes Kallel)

Abstract: Nano-sized Y- Ag doped and co-doped TiO₂ particles were synthesized using the sol-gel method and Ti(OBu)₄ as TiO₂ precursor. Their structural and optical properties were examined by scanning electron microscopy (SEM), XRD, thermogravimetric-differential thermal analysis (TG-DTA), FT-IR and UV-vis absorption spectroscopies. The photocatalytic activity of these materials was investigated for the photodegradation of methylene blue (MB) as a model reaction under visible light irradiation. Ground state diffuse reflectance absorption studies reveal that both Y and Ag dopant cause deviations of the band gap to higher energies attesting that co-doping the TiO₂ with Y and Ag could enhance the photocatalytic activity by delaying the electron-hole recombination by means of higher energy band gaps. Co-doping TiO₂ at a level of 4% (Y, Ag) samples leads to a significant decrease in the crystallite size of photocatalyst and containing both anatase and Ag/AgCl components. However, the high photocatalytic performance is attributed to an efficient electron-hole pairs separation at the photocatalyst interfaces in addition to localized surface plasmon resonance of Ag particles. The development of these visible light- activated nanocatalysts has the potential of providing environmentally benign routes for water treatment.

Keywords: titanium dioxide, XRD, plasmonic photocatalyst, methylene blue, visible light

1. Introduction

Various pollutants such as dyes, pesticides, insecticides and industrial chemicals made water unfit for consumption (Ahmed et al., 2010; Hoffmann et al., 1995). These pollutants have been found to be unwholesome to animals, human beings and the environment (Shahmoradi et al., 2011; Ahmed et al., 2010; Binitha et al., 2009; Molinari et al., 2004). Hence, there is an urgent need to detoxify the hazardous pollutants by an environmentally greener method. Among them, photocatalytic degradation has been recommended as potential and the cheapest route to detoxify the various injurious organic compounds (Atchudan et al., 2017; Jebakumar et al., 2016; Ibadon and Fitzpatrick, 2013).

At the present time, titanium dioxide (TiO₂) has been commercially used in many applications including dye synthesised solar cells (DSSCs) (Liang et al., 2013), water splitting (Freitas et al., 2014), self-cleaning (Murugan et al., 2013), and water purification (Nakata et al., 2012) due to its strong oxidizing behaviour, good photocatalytic activity, chemical stability, and non-toxicity. When illuminated by light of energies greater than the band-gap energy (3.2 eV), TiO₂ shows strong oxidation capacity, which can oxidize almost all organic compounds to CO₂ (Jingxiang et al., 2017). However, TiO₂ suffers from a few critical issues to be applied as a photocatalyst. The absorption of solar light by TiO₂ is limited due to its wide band gap which means that TiO₂ can be sensitive only to UV region that covers less than 5% of the total solar spectrum. Another hurdle is that the recombination time of electron-hole pairs is very short ($\sim 10^{-9}$ s) compared to the chemical interaction time ($\sim 10^{-3}$ - 10^{-8} s) between the TiO₂ surface and adsorbed dyes or other molecules, which may pose certain constraints on the performance (Lavanya et al., 2014). In order to overcome these difficulties, numerous efforts have been dedicated to ameliorate the photocatalytic activity of TiO₂ such as doping with non-metal or metal ions, loading of

noble metals and making composite with metal oxides (Slimen et al., 2015). Dopants may play a key role in the photoreaction by synergistic reaction, which is essentially different from the role of one single doping ion. To the best of our knowledge, there are few studies carried out on TiO₂ nanoparticles co-doped with two kinds of ions.

In this study, Y ions have been chosen as dopant because rare earths are extremely useful in various applications due to their sharp, near monochromatic emission lines. Furthermore, the f-f transitions are fairly insensitive to conditions such as temperature and the surrounding chemical environment (Ballato et al., 1999; Hufner, 1978). The use of Rare earth ions such Ln = Eu, Pr, La, Pr, Nd (Parida and Sahu, 2008), as dopants for crystalline TiO₂ can lead to the incorporation of atoms/ions of these elements into TiO₂ crystalline matrices, or to a surface modification. This can adduce a potential means to inhibit the combination of photo electron-hole pairs, enlarge the light adsorption of the semiconductor and therefore enhance the visible light photocatalytic activity. On the other hand, noble metal nanoparticles such as Ag, Au and Pt exhibit plasmonic characteristics through electron transfer (Huang et al., 2016a; Huang et al., 2016b; Huang et al., 2015). Among these noble metals, silver is mostly used because of its low toxicity, bactericidal capability, relatively low cost compared to other noble metals. Recently, localized surface plasmonic resonance (LSPR) of silver metals shows significant pledge in enlarging the absorption scope of TiO₂ (Ruirui et al., 2018; Jiang et al., 2014). Unlike the traditional Ag/semiconductor plasmonic systems, silver halide materials (AgX, X = Cl, Br and I) exhibit good stability even after the preliminary decomposition into Ag⁰ species under irradiation (Liu et al., 2013) and are, therefore, found to be one of the most promising plasmonic photocatalysts (Cai et al., 2014) with stellar photocatalytic performances under visible light irradiation (Hajjaji et al., 2018; Ma et al., 2016).

As an excellent conductor, Ag can availably capture photogenerated electrons and promote electron-hole separation to restrain electron-hole recombination (Huijun et al., 2018; Wen et al., 2015). Consecutively, this electron transferred from Ag to the conduction band of TiO₂ is captured by oxygen turning into O₂^{•-} (An et al., 2016; Kowalska et al., 2010), which can oxidize organic molecules. Wang et al. (2013) synthesized TiO₂ nanofibers modified by Ag/AgCl to promote highly efficient and stable visible light photocatalytic activities for the degradation of 17- β -ethinylestradiol. Guo et al. (2012) found that the modification of TiO₂ with Ag/AgCl obviously showed enhanced photocatalytic degradation of 4-CP and photoreduction of Cr(VI) under visible light irradiation, due to the LSPR of Ag and the coexistence of Ag and AgCl.

Although the SPR effect of silver and silver halide makes it feasible to synthesize a new type of active, stable photocatalyst by combining the advantages of silver and silver halide nanoparticles with TiO₂, this combination may bring to the synergistic effect of SPR structural defects which will improve the visible light induced photocatalytic performance.

In this paper, we report a detailed investigation into co-doping varying amounts of yttrium and silver into TiO₂ powders aiming at an understanding on their effects on the structural orderliness, nanocrystallinity and photocatalytic properties using three dyes aqueous solutions as model organic pollutant under visible-light irradiation.

2. Experimental methods

2.1. Powder preparation

In this work, the preparation of the sample was conducted using sol-gel process. The experimental process involved two steps: X% doped and co-doped samples were prepared using the following materials: YCl₃ · 6H₂O, Ti(OBu)₄ and AgNO₃ (all of them from Aldrich) where X is the molar ratio ($X = n_d/n_{Ti}$), with $X = 0.5, 1, 2, 3, 4, 5$ and $n_d = n_{Ag}$ or n_Y). In order to adjust the proportions of (Ag or/and Y) and TiO₂ in a typical experiment for the synthesis of 3%, designated as 3% Ag doped TiO₂, 3% Y doped TiO₂ and 3% Y-Ag co-doped TiO₂ the values of X were set to: 3, 97, 0; 0, 97, 3 and 3, 94, 3, respectively.

AgNO₃ was dissolved in absolute ethanol with constant stirring to get a clear solution. Then, it was added to YCl₃ · 6H₂O dissolved in acetic acid, which act as a solvent and hydrolysis promoter. To this mixture, a solution of Ti(OBu)₄ was introduced progressively and kept under magnetic stirring at 80°C temperature until gelation occurs. The final product was dried at 100 °C for 24 h and stored at room

temperature for use as starting material in this study. This procedure gives rise mesoporous solids, which are initially amorphous and crystallize upon further heating above 400°C within 2 hours.

2.2. Experimental techniques

Scanning electron microscopy (SEM) studies were performed using a Philips XL30 CP microscope equipped with EDX (energy dispersive X-ray), Robinson, SE (secondary electron) and BSE (back-scattered electron) detectors. The sample was placed on an adhesive C slice and coated with Au-Pd alloy 10 nm thick layer.

The XRD patterns were recorded using Siemens D5000 X-ray diffractometer. The powder X-ray diffraction data were collected at ambient temperature over the range $10 < 2\theta < 60^\circ$ by step scanning, using 2θ increments of 0.02° to determine the crystallographic phases. The crystallite size was determined from the broadening of corresponding X-ray spectral peaks by Scherrer formula (Qinghong et al., 2000):

$$L = K\lambda / (\beta \cos\theta) \quad (1)$$

where L is the crystallite size, λ is the wavelength of the X-ray radiation ($\text{CuK}\alpha = 0.15418 \text{ nm}$), K is the usually taken as 0.89, and β is the line width at half-maximum height. This is the generally an accepted method to estimate the mean crystallite size of nanoparticle.

Infrared spectra were recorded with a Varian 7000 FT-IR spectrometer with a DTGS coupled detector. Samples were analysed in transmittance mode. Spectra were recorded at 1.0 cm^{-1} resolution in the $4000\text{--}400 \text{ cm}^{-1}$ range as a ratio of 16 single-beam scans of the sample to the same number of background scans using dry air in the sample compartment. No baseline corrections were introduced. The original samples were mixed with KBr (about 2% wt./wt.) and ground, with the use of an agate mortar and pestle, to form a finely divided powder.

Differential thermal analysis (DTA) and thermo-gravimetric analysis (TGA) runs of the xerogels were carried out in a SETARAM92 TGA-DTA. Samples were heated from 25 to 500 °C under synthetic air (20% vol. of O_2 and 80% vol. of N_2) at 5°C min^{-1} .

Ground-state absorption studies were performed using all powdered samples, by means of an OLIS14-VIS-NIR spectroscopy operating system with diffuse reflectance. The reflectance (R) from each sample was obtained by scanning the excitation monochromator from 240 to 840 nm, and the remission function $F(R)$ was calculated using the Kubelka–Munk equation for optically thick samples (those where no further increase of the sample thickness can change the experimentally determined R). The remission function, according to Ferreira et al. (1998) is:

$$F(R) = (1-R)^2 / 2R \quad (2)$$

2.3. Photocatalytic activity measurements

This work reports on the synthesis of Y or/and Ag doped TiO_2 nanoparticles using the sol-gel process, and investigates their potential use as a photocatalyst for degradation under visible excitation. Three different dyes: methylene blue (Color Index (CI): 52015), methyl red (CI: 13020) and methyl orange (CI: 13025) were used as model organic pollutants (Fig. 1) in aqueous solution. In each of the experiments, 0.05 g of catalyst and 50 cm^3 of approximately $10^{-4} \text{ mol L}^{-1}$ solutions of the organic dye were prepared. Then finely powdered doped titanium dioxide was added as a photocatalyst and shaken vigorously to form a homogenous mixture. In each case, the mixture was sonicated (bath sonicator) before irradiation for 10 min to obtain highly dispersed catalysts. Before irradiation, solutions were maintained in the dark for 1h in order to achieve the maximum adsorption of organic pollutant on the photocatalyst surface. The degradation tests were carried out under irradiation by a halogen lamp of power 42 W (230 V) and emitting light with λ varying between 380 and 780 nm (Scheme 1).

The aqueous suspension was kept under magnetic stirring during the entire reaction period to maintain the suspension homogeneity. At constant time intervals, 2 mL aliquots were sampled, immediately centrifuged at 24000 rpm for 15 min to remove the TiO_2 particles, and then analyzed on a Cecil UV-visible spectrophotometer. The UV absorbance of the solutes was measured at their corresponding λ_{max} . Calibration curves were previously established for each solute studied here. A 54

W Halogen lamp was used as visible light source. The use of a lamp assures a constant light output in opposition to the fluctuation in solar intensity with season and time of day.

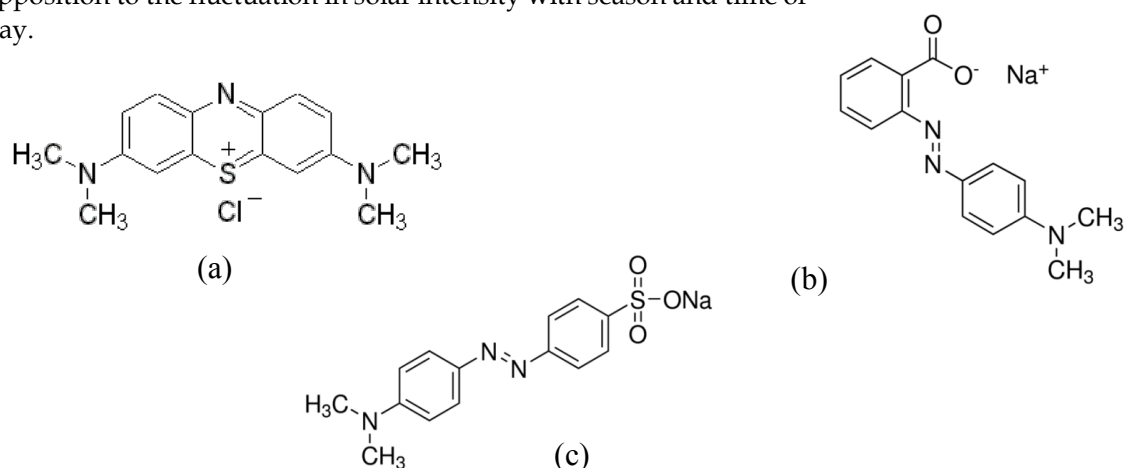


Fig. 1. Molecular structure of (a) methylene blue (b) methyl red and (c) methyl orange



Scheme 1. Photocatalytic reactor using a halogen lamp as a source of irradiation

3. Results and discussion

3.1. EDX analysis

EDX observations have been carried out for 4% (Y,Ag) co-doped TiO₂ sample calcined at 400°C. As shown in figure Fig. 2, the EDX analysis confirmed the presence of all the desired elements even those used at a small level: O, Cl, Ti, Ag and Y. Additionally, one can show that, in the 4%(Y, Ag) co-doped TiO₂ photocatalysts, the Ag amount is slightly higher than that of Cl. It can be inferred that the surface atomic ratio of silver to chlorine was higher than the stoichiometric ratio in AgCl (1:1), indicating probably the existence of Ag on the surface of our sample.

3.2. XRD characterization

XRD was used to investigate the phase structure of the prepared samples. XRD patterns of the Y doped and Ag doped titania with different concentrations, after calcinations at 400°C, are superimposed in Fig. 3. The XRD pattern of pure TiO₂, Y doped TiO₂ and Ag doped TiO₂ powders shows seven distinctive TiO₂ reflections corresponding to the anatase tetragonal structure (I4₁/amd) (Sanchez et al., 1996). No peak due to rutile or other titania phase can be detected in all samples.

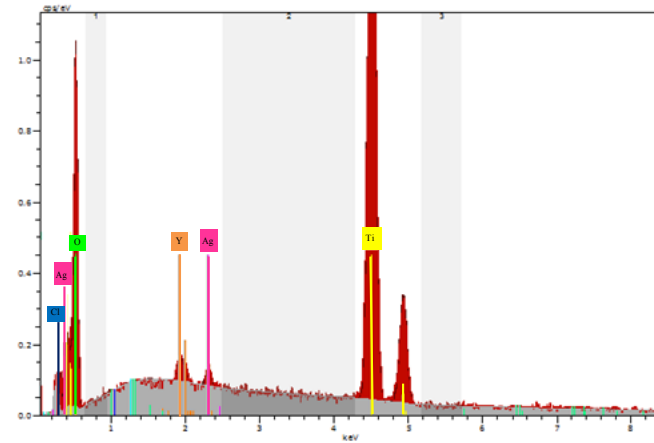


Fig. 2. The energy dispersive X-ray spectra of 4% (Y, Ag) co-doped TiO_2 , calcined at 400°C

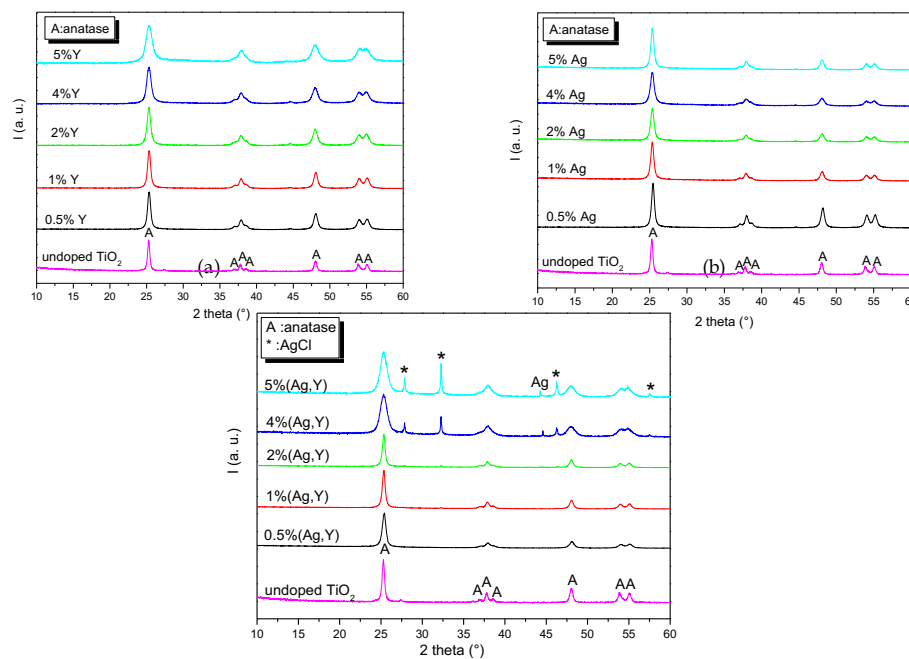


Fig. 3. XRD patterns of undoped, (a) X% Y doped TiO_2 ($X=0.5, 1, 2, 4$ and 5), (b) X% Ag doped TiO_2 ($X=0.5, 1, 2, 4$ and 5) and (c) X% (Y,Ag) co-doped TiO_2 ($X=0.5, 1, 2, 4$ and 5) calcined at 400°C

Figure 3c shows the diffractogram of (Y,Ag) co-doped TiO_2 samples calcined at 400°C . At this temperature anatase is the only observed phase for 0.5%, 1% and 2% (Y,Ag) co-doped samples. However, the diffractogram of 4% and 5% (Y, Ag) co-doped TiO_2 powders show four additional peaks. All of them are attributed to cubic AgCl phase (JCPDS No.85-1355). Moreover, a careful analysis of the diffractogram of two samples reveal the presence of another small reflection at 44.6° assigned to Ag-containing phase. The presence of Ag and AgCl ultimately did not modify the position of the main reflection (101) of the anatase phase. Compared to pure TiO_2 the XRD reflections of doped and co-doped TiO_2 samples have the same positions, suggesting that Ag^+ and Y^{3+} did not enter TiO_2 crystalline lattice to substitute Ti^{4+} . Ionic radius and calcinations temperature are two important parameters, which strongly influence the ability of the dopant to enter into the TiO_2 crystalline lattice to form stable solid solution. If the ionic radius of the doping ion is much larger, the substitution process can be suppressed (Jun and Jimmy, 1998). The relatively huge difference between the Ti^{4+} (0.64 \AA) radius and those corresponding to Y^{3+} (0.95 \AA) and Ag^+ (1.15 \AA) rationalize that such substitution with Ag^+ and Y^{3+} couldn't occur. They are adsorbed at the surface of the TiO_2 particles. On the other hand, the widening of the reflections can be due to a systematic decrease in grain size. The average size of crystallites

determined by Sherrer formula of Y doped, Ag doped and (Y,Ag) co-doped TiO₂ are illustrated in Table 1.

Table 1. Crystallite size of the Y-Ag doped and co-doped TiO₂ anatase samples

Doping rate	Dopants	Crystallite size (nm)
0%	-	25
0.5%	Y	20
	Ag	19
	Y-Ag	16
1%	Y	13
	Ag	18
	Y-Ag	15
2%	Y	12
	Ag	17
	Y-Ag	13
4%	Y	9
	Ag	16
	Y-Ag	7
5%	Y	8
	Ag	13
	Y-Ag	8

It is clear from all these results that the presence of dopants Ag or/and Y inhibit the growth of TiO₂ particles and justify the decreasing of anatase grain size, especially for 4% (Y,Ag) and 5% (Y,Ag) co-doped TiO₂ sample.

3.3. Thermal analysis study

Figure 4 shows the TGA-DTA curves of dry 4% (Y,Ag) co-doped TiO₂ xerogel, respectively. It can be found that there are mainly two steps during the weight loss process. The first step corresponds to a weight loss of about 7% at the temperature range from the room temperature to 140 °C accompanied by a small decalescence band at 73 °C in the DTA curve, which is originated mainly from the reorientation and evaporation of adsorbed water. The second weight loss is observed in the temperature domain 250-450 °C corresponding in the DTA curves in one releasing thermal peak at 350 °C. It can be attributed to different phenomena: (i) the removal of structural hydroxyls, which will increase the number of bridging oxygens, (ii) the thermal oxidation of organic groups and (iii) the phase transition of TiO₂ xerogel from amorphous to anatase and the formation of AgCl phases in the 4% (Y,Ag) co-doped TiO₂.

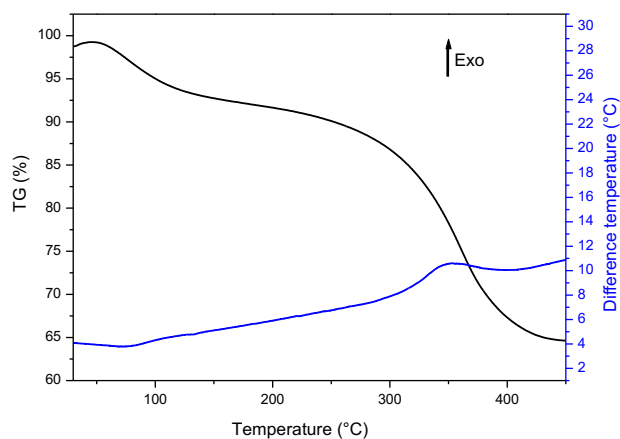


Fig. 4. TG-DTA curves of 4% (Y, Ag) co-doped TiO₂ xerogel

3.4. FT-IR studies

FTIR studies were performed in order to determine the presence of functional groups as well as to study the structural changes in the TiO₂ semiconductor after incorporation of dopants. Figure 5 presents the FT-IR absorption spectra in the 400–4000 cm⁻¹ region, for the 4% Y-Ag doped and co doped TiO₂ samples, annealed at 400°C. The presence of OH groups and water at the surface of the system is evidenced by the appearance of a broad band at about 3440 cm⁻¹ accompanied by another peak around 1630 cm⁻¹ for all samples. They are from Ti–OH stretching modes. However, it can be seen through the increase in the intensity of the band around 1632 cm⁻¹ that addition of AgCl to TiO₂ in 4% (Y,Ag) enhanced the concentration of OH radicals on TiO₂ surface. These titanol groups can establish hydrogen bonds with organic pollutants, improve the adsorption and enhance the photodegradation performance. The stretching vibration of –CH₂ of the residual butyl titanate appeared at 1162 cm⁻¹ (Li et al., 2013). All the samples show a shoulder at 980 cm⁻¹. This is attributed to the anatase Ti–O bond (Tayade et al., 2007), which is formed during gelation at room temperature itself. The undoped sample shows two peaks at 520 and 663 cm⁻¹, which is the characteristic peak of titania. But in the case of Y-Ag doped and co-doped TiO₂ samples these peaks are shifted to a large frequency that exists between 410 and 900 cm⁻¹, which may be due to the formation of Ti–O–Ag and Ti–O–Y (Vargas et al., 2015).

3.5. Ground state diffuse reflectance spectra

Ground state diffuse reflectance spectra were used to probe the band structure (or molecular energy levels) in the materials since UV–vis light excitation creates photogenerated electrons and holes. The UV–vis reflectance band edge is a strong function of nanoparticle titania cluster size, which can be attributed to the well-known quantum-size effect for semiconductors (Zhou et al., 2006). The corresponding UV–vis diffuse reflectance spectra of the pure TiO₂ and (Y,Ag) co-doped TiO₂ samples are superimposed in Fig. 6. The reflectance edge shifts toward shorter wavelengths for (Y,Ag) co-doped TiO₂ powders compared to undoped spectra. This indicates an increase in the band gap energy of TiO₂ (Table 2). These results are compatible with the existence of very small nanoparticles in the powders, leading to strong quantum confinement effects responsible for the high energy gaps (Xue et al., 2012). The band gap energy values for the different samples were calculated according to the transformed Kubelka-Munk function (Simmons, 1975).

The analysis of the results reveals that the values of the energy gap depend on the co-doping levels. Ground state diffuse reflectance absorption studies for the nanopowders show that the (Y,Ag) co-dopant causes deviations of the band gap to higher energies (Table 2) revealing that doping the TiO₂ with Y and Ag could enhance the photocatalytic activity of the sample, while delaying the electron-hole recombination by means of higher energy band gaps. Moreover, an additional broad absorption is observed, for 4% and 5% (Y,Ag) co-doped sample, in the visible region of 450–650 nm, which could be due to surface plasmon resonance of the Ag nanoparticles produced by the photoreduction of AgCl (Jingxiang et al., 2018; Liang et al., 2015).

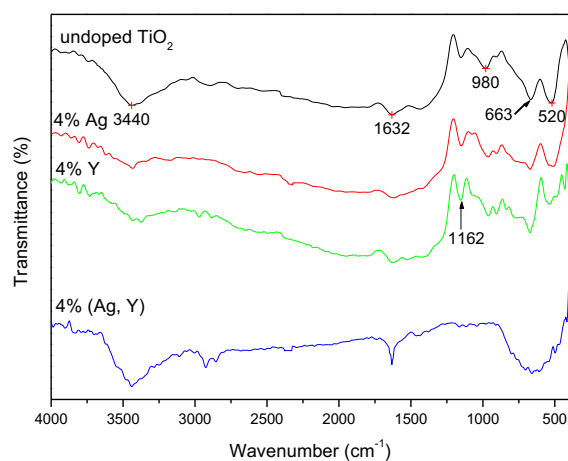


Fig. 5. FTIR spectra of undoped, Y-Ag doped or co-doped TiO₂ samples annealed at 400°C

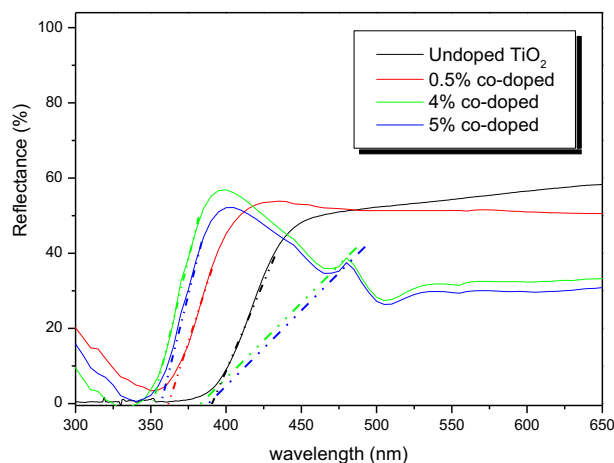


Fig. 6. DR spectra of undoped and co-doped TiO₂ with Y and Ag

These experimental results are in agreement with the data reported by Yin et al. (2016), indicating that AgCl phase present in 4% and 5% (Y,Ag) co-doped sample has potential ability for photocatalytic decomposition of organic contaminants under visible light irradiation. The analysis of the results reveals that the values of the energy gap depend on the co-doping levels. Ground state diffuse reflectance absorption studies for the nanopowders show that both the Y and Ag dopant cause deviations of the band gap to higher energies (Table 2) revealing that doping the TiO₂ with Y and Ag could enhance the photocatalytic activity of the sample, while delaying the electron-hole recombination by means of higher energy band gaps.

Table 2. Energy gaps of undoped, Y and Ag co-doped TiO₂

Samples	E _g (eV)
Undoped TiO ₂	3.18
0.5% (Y,Ag)	3.42
4% (Y,Ag)	3.51
5% (Y,Ag)	3.46

3.6. Photocatalytic degradation

Given the serious health risks associated with the presence of dyes in the environment, predominantly in the aqueous phase, and taken into account results obtained by ground state diffuse reflectance, it should be emphasized that using Y-Ag doped and co-doped TiO₂ which have an important absorption in the visible light as photocatalysts can be very interest. To identify the role of each chemical species a comparison on the photocatalytic efficiency of single doping and co-doping materials, under visible light excitation was investigated using three model organic dye pollutants.

As shown in Fig. 7, MB cannot be degraded in the absence of catalyst and under dark. Additionally, in the presence of undoped TiO₂, 78% of the MB remained in the solution after 12 h of exposure, attesting the low photocatalytic activity of this sample under visible irradiation. Doping TiO₂ with Y or Ag notably affects the photocatalytic activity. However, the largest catalytic effect is observed in the presence of 5% Ag for which the residual concentration of MB attained 39% after 12 h of visible light irradiation. One should note that, all of the samples used in the present study are in the anatase form, their photocatalytic activities differ considerably. This rules out the assignment of the difference in the degradation efficiency to the structural properties. However, this result can probably be explained by the fact that, using sol-gel approach, the Ag dispersed on the TiO₂ surface, favoring its surface enrichment and yielding low average distances between the Ag particles and the TiO₂ ones (Bo-Kyung et al., 2018; Bouattour et al., 2010).

On the other hand, using Y and Ag as co-doping elements leads to higher photocatalytic performances (Fig. 7c). One can evoke the contribution of the adsorption at the surface of the photocatalyst to account for the drop in the solute concentration with time. However, this hypothesis could be ruled out given the low conversion attained in the dark with a concentration ratio reaching only 93% for MB in the presence of 4% (Y,Ag), which indicated that there was no degradation when irradiation was absent. As shown in Figure 7c the highest activity was not observed for pure anatase but for 4% (Y,Ag) sample which is composed of two phases: TiO₂ anatase and AgCl as proved by XRD analyses. Nanoparticles of Ag were also evidenced. In the presence of this photocatalyst, a strong improvement of the photocatalytic activity was noticed with complete MB degradation after 12 h of exposure to visible irradiation. This results suggest that some synergism between anatase and Ag/AgCl exists leading to faster degradation rates of MB.

Taken into account the different component of the system and owing to the plasmon response effect, Ag⁰ particles propels the 4% (Y,Ag) sample to absorb visible-light, which has been demonstrated by UV-vis DRS analysis. Plasmonic enhancements and facile charge transfer resulting from the assistance of metallic Ag are proposed to explain the high photocatalytic activity of the 4% (Y,Ag) co-doped TiO₂ photocatalysts. In previous studies (Qi et al., 2014; Wang et al., 2013), it has been demonstrated that the plasmonic effect of Ag⁰ particles plays a very important role in producing high visible light photocatalytic activity due to the oscillation of surface electrons. Additionally, the rich conduction band (CB) electrons of noble metals can enhance the reducibility of the sample, resulting in a decreased recombination opportunity of electrons and holes (Pham et al., 2014). In particular, the excellent conductivity of Ag nanoparticles greatly promotes interfacial charge transfer kinetics among Ag, AgCl, and TiO₂.

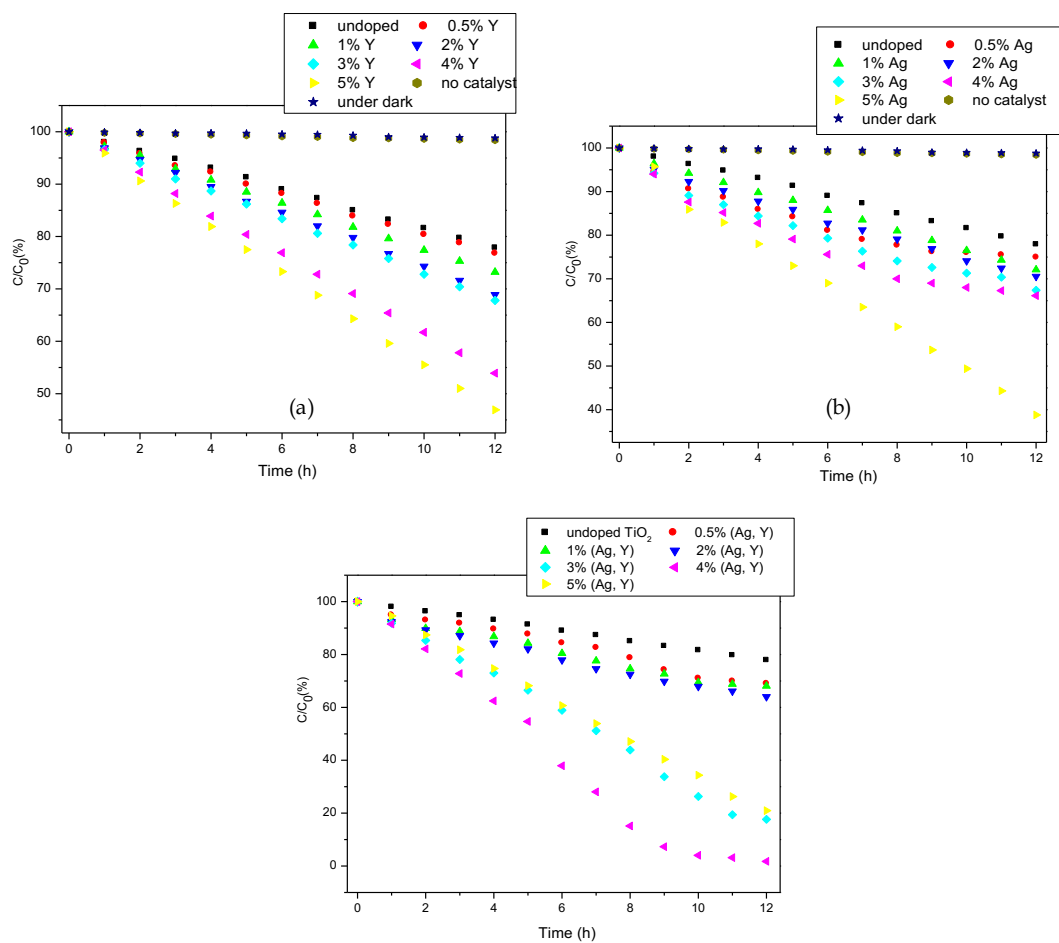


Fig. 7. Evolution of the concentration of MB vs time in the presence of (a) TiO₂ doped with Y-doped, (b) TiO₂ doped with Ag and (c) TiO₂ co-doped with Y and Ag under visible light excitation

This study demonstrates that an optimal amount of 4% (Y,Ag) co-doping can effectively increase the photocatalytic performance of TiO₂ and will promote the photocatalytic degradation of MB. The effect of these phases in the 4% (Y,Ag) co-doped TiO₂ catalyst on the photocatalytic efficiency under visible light excitation was also investigated using methyl orange and methyl red as a model pollutants. However, a careful analysis of Fig. 8 reveals that the better photodegradation performance is observed for MB compared to methyl orange and methyl red. In fact, after 12 h exposure, the residual concentration ratio attains about 44, 37 and 1% for methyl red, methyl orange and methyl blue, respectively. The degradation rate of the first two organic dyes, using 4% (Y,Ag) co-doped TiO₂ powder as photocatalyst, is quite low as compared to MB. These results can be explained by the fact that the conversion profile is dependent on the structure of the organic pollutant. The higher efficiency observed for the MB is probably a consequence of the high adsorption capacity of this compound on 4% (Y,Ag) catalyst which is the prerequisite step for the occurrence of the degradation process (Gaya et al., 2008).

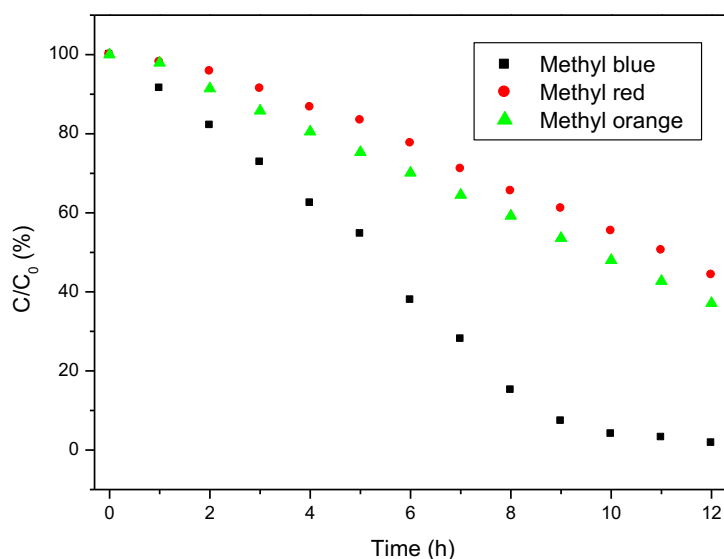


Fig. 8. Evolution of the residual concentration of the organic dye vs. time, in the presence of TiO₂ co-doped with 4% (Y,Ag) under visible irradiation

3.7. Kinetic study

Kinetics of the degradation reaction of aqueous solution of MB pollutant was also investigated. Indeed, the photodegradation results of photocatalyst obey pseudo-first-order kinetics over the time period investigated and the slope equals the apparent degradation rate constant (K_{app}). This is in an agreement with the generally observed Langmuir-Hinshelwood mechanism. It basically relates the degradation rate and reactant concentration C , in water at time t . When the adsorption is relatively weak and/or the reactant concentration is low, the system can simplify to a pseudo- first-order kinetics with an apparent first-order rate constant

$$\ln\left(\frac{C}{C_0}\right) = -K_{app} \times t \quad (3)$$

where C_0 is the initial organic dye concentration. For all catalysts, plotting $\ln(C/C_0)$ vs. reaction time t yields a straight line, and the slope is the apparent rate constant. Table 3 show the apparent rate constants K_{app} and regression coefficients R^2 for the photodegradation of MB in the presence of Y doped, Ag doped and (Y,Ag) co-doped TiO₂ catalysts. From the data reported in Table 3, the trend in the value of K_{app} is in line with the enhancement in the photocatalytic activity. Kinetics of MB degradation, in presence of 4% (Y,Ag) co-doped TiO₂ catalyst, leads to a K_{app} value of 0.348 h⁻¹.

This value is very high as compared to those observed for the others catalysts attesting the fast MB decolorization in presence of this catalyst. This result confirmed the improved efficiency in photocatalytic activity observed by adding Ag/AgCl to TiO₂.

Table 3. Apparent first-order rate constant K_{app} and correlation coefficient R^2 for photodegradation of MB by undoped and (Y,Ag) doped TiO_2 under visible light excitation.

Doping rate	Dopants	$K_{app} \times 10^3$ (h^{-1})	R^2
0%	-	21	0.99
0.5%	Y	21	0.99
	Ag	23	0.98
	Y-Ag	31	0.97
1%	Y	25	0.98
	Ag	26	0.99
	Y-Ag	32	0.98
2%	Y	30	0.99
	Ag	27	0.99
	Y-Ag	35	0.99
3%	Y	31	0.99
	Ag	30	0.98
	Y-Ag	146	0.97
4%	Y	50	0.99
	Ag	34	0.97
	Y-Ag	348	0.99
5%	Y	62	0.99
	Ag	75	0.98
	Y-Ag	125	0.98

3.8. Reuse of photocatalyst

The aptitude of a photocatalyst to be reused is one of the most important parameters which determine, from an economical point of view, the potential exploitation of a material in practical systems for water treatment. To examine the repeatability of the photocatalytic activity, the 4% (Y,Ag) co-doped TiO_2 sample was used for three consecutive photodegradation cycles. The concentration of the MB was measured after 12 h exposition to visible irradiation (Fig. 9). After each decomposition reaction, the TiO_2 powder was separated and used again in the same conditions. It can be seen from Fig. 11 that the photocatalytic efficiency decreases slightly after three degradation cycles of degradation. It is worthy to note that the reused powder was used without washing or any purification treatment. The residual concentration of MB attained 1, 11 and 17 % after three degradation cycles. This result may be explained by the formation of some by-products and their accumulation on the active surface sites of the photocatalyst, thus making the active site on the surface less available.

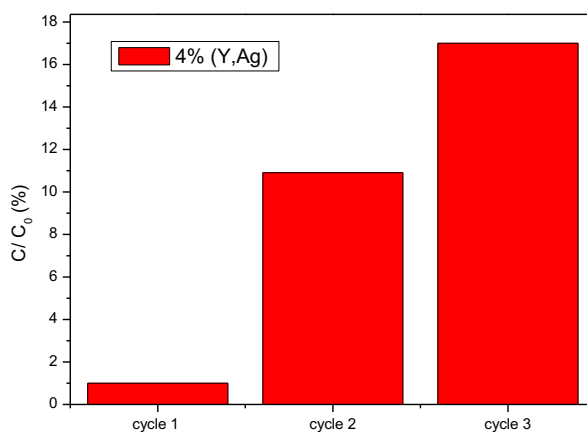
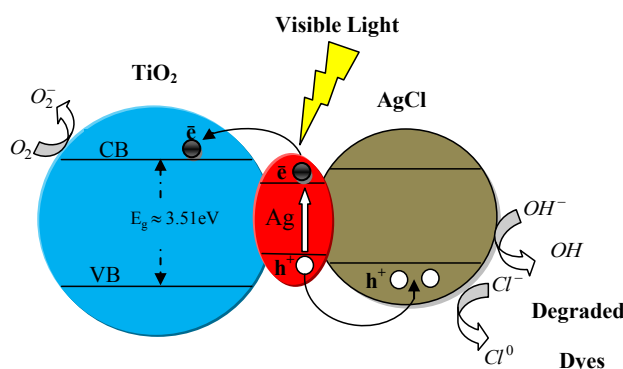


Fig. 9. Evolution of the residual concentration of the MB after 12 h, in the presence of 4% (Y,Ag) co-doped TiO_2 under visible light excitation

3.9. Mechanism of electron transfer in 4% (Y,Ag) co-doped TiO₂ catalyst

The surface plasmon resonance character of metallic Ag, Ag⁰ can absorb visible light, and the absorbed photon will lead efficiently to the separation of electron and hole charges. The AgCl present in the system also acts as a hole acceptor (Yao and Liu, 2014). In fact, the holes transferred to the AgCl surface, results in the oxidation of Cl⁻ ions to Cl⁰ atoms (Cui et al., 2013). The formed Cl⁰, participates as reactive species for the oxidation of dye molecules. Meanwhile, more holes with strong oxidation power in the VB can be trapped by OH⁻ to form hydroxyl radicals, which participates in the MB degradation. On the other hand, the plasmon induced electrons of Ag nanoparticles are transported to the CB of TiO₂ (Liang et al., 2014) and trapped by absorbed O₂ to produce O₂⁻, which is the active specie in the degradation reaction of pollutant. All of this result can explain the high performance of Ag/AgCl-TiO₂ photocatalysts under visible light irradiation. A schematic illustration of effective separation and instant scavenging of photoexcited electron-hole pairs in the Ag/AgCl-TiO₂ is presented in Scheme 2.



Scheme 2. Photocatalytic mechanism behaviour of 4% (Y,Ag) co-doped TiO₂ sample under visible light irradiation

It is important to precise that visible-light absorption of dye molecules can also contributes in the photocatalytic process since photo-excited electrons can be efficiently transferred from dyes to TiO₂. As a result, the dyes are converted to a cationic radical (dye^{+•}), and [•]O₂⁻ radical specie were easily formed by the adsorbed oxygen, through capturing electrons from the conduction band of the catalyst. The [•]O₂⁻ can react with surface adsorbed H₂O to form H₂O₂ which is ultimately converted to [•]OH (Turkten and Cinar; 2017).

4. Conclusion

In the present work, Y-Ag doped and co-doped TiO₂ particles were successfully prepared and their photocatalytic performance under visible irradiation was investigated using MB as a model pollutant. Y-Ag co-doped TiO₂ increased the energy band gap of the semiconductor, simultaneously, the electron/hole recombination is delayed by means of the higher band gap.

Results showed a significant enhancement of the photocatalytic activity, especially, for 4% (Y,Ag) co-doped TiO₂ samples, with very small nanoparticles, containing both anatase and Ag/AgCl catalyst. This improvement is attributed to the existence of a synergistic effect between anatase and Ag/AgCl leading to a better separation between photogenerated electrons and holes. The high photocatalytic activity of the 4% (Y,Ag) co-doped TiO₂ compound results from efficient electron-hole pairs separation at the interfaces and role of localized surface plasmon resonance of Ag particles formed on AgCl particles in the degradation reaction.

References

AHMED, S., RASUL, M.G., MARTENS, W.N., BROWN, R., HASHI, M. A., 2010. *Heterogeneous photocatalytic degradation of phenols in wastewater: a review on current status and developments*. Desalination 261, 3-18.

- AN, C.H., WANG, S.T., SUN, Y.G., ZHANG, Q.H., ZHANG, J., SIU, C., WANG, C.Y., FANG, J.Y., 2016. *Plasmonic silver incorporated silver halides for efficient photocatalysis*. J. Mater. Chem. A, 4, 4336–4352.
- ATCHUDAN, R., JEBAKUMAR, I.E.T.N., PERUMAL, S., SHANMUGAN, M., LEE, Y.R., 2017. *Direct solvothermal synthesis of zinc oxide nanoparticle decorated graphene oxide nanocomposite for efficient photodegradation of azo-dyes*. J. Photochem. Photobiol. A: Chem. 337, 100–111.
- BALLATO, J., LEWIS, J.S., HOLLOWAY, P., 1999. *Synthesis and luminescence properties of mesostructured thin films activated by in-situ formed trivalent rare earth ion complexes*. MRS Bull. 24, 51–56.
- BINITHA, N., NARAYANAN, Z.Y., RANJANA, K., SOUMINI, C., SANKARAN, S., FEMINA, K.S., VINEETHA, M., 2009. *Photodegradation of methyloange over zirconia doped TiO₂ using solar energy*. Eur. J. Sci. Res. 28, 566–571.
- BO-KYUNG, C., WOONG-KI, C., SOO-JIN P., MIN-KANG S., 2018. *One-pot synthesis of Ag-TiO₂/nitrogen-doped graphene oxide nanocomposites and its photocatalytic degradation of methylene blue*. J. Nanosc. Nanotech. 18, 6075–6080.
- BOUATTOUR, S., KALLEL, W., DO REGO, A.M.B., FERREIRA, L.F.V., MACHADO, I.F., BOUFI, S., 2010. *Li-doped nanosized TiO₂ powder with enhanced photocatalytic activity under sunlight irradiation*. Appl. Organomet. Chem. 24, 692–699.
- CAI, B., WANG, J., GAN, S., HAN, D., WU, Z., NIU, L., 2014. *A distinctive red Ag/AgCl photocatalyst with efficient photocatalytic oxidative and reductive activities*. J. Mater. Chem. A, 2, 5280–5286.
- CUI, W., WANG, H., LIU, L., LIANG, Y., MCEVOY, J.G., 2013. *Plasmonic Ag@AgCl-intercalated K₄Nb₆O₁₇ composite for enhanced photocatalytic degradation of Rhodamine B under visible light*. Appl. Surf. Sci. 283, 820–827.
- FERREIRA, L.F.V., CABRAL, P.V., ALMEIDA, P., OLIVEIRA, A.S., REIS, M.J., BOTELHODO, R.A.M., 1998. *Ultraviolet/visible absorption, luminescence and X-ray photoelectron spectroscopic studies of a rhodamine dye covalently bound to microcrystalline cellulose*. Macromolecules 31, 3936–3944.
- FREITAS, R.G., SANTANNA, M.A., PEREIRA, E.C., 2014. *Preparation and characterization of TiO₂ nanotube arrays in ionic liquid for water splitting*. Electrochim. Acta. 136, 404–411.
- GAYA, U.I., ABDULLAHA, A.H., 2008. *Heterogeneous photocatalytic degradation of organic contaminants over titanium dioxide: A review of fundamentals, progress and problems*. J. Photochem. Photobiol. C, 9, 1–12.
- GUO, J., MA, B., YIN, A., FAN, K., DAI, W., 2012. *Highly stable and efficient Ag/AgCl@TiO₂ photocatalyst: preparation, characterization, and application in the treatment of aqueous hazardous pollutants*. J. Hazard. Mater. 211–212, 77–82.
- HAJJAJI, A., ELABIDI, M., TRABELSI, K., ASSADI, A.A., BESSAIS, B., RTIMI, S., 2018. *Bacterial adhesion and inactivation on Ag decorated TiO₂-nanotubes under visible light: Effect of the nanotubes geometry on the photocatalytic activity*. Coll. Sur. B: Biointer. 170, 92–98.
- HOFFMANN, M.R., MARTIN, S.T., CHOI, W.I., BAHNEMANN, D.W., 1995. *Environmental applications of semiconductor photocatalysis*. Chem. Rev. 95, 69–96.
- HUANG, Y.B., WANG, Q., LIANG, J., WANG, X., 2016a. *Soluble metal-nanoparticle-decorated porous coordination polymers for the homogenization of heterogeneous catalysis*. J. Am. Chem. Soc. 138, 10104–10107.
- HUFNER, S., 1978. *Optical spectra of transparent rare earth compounds*. Academic Press. New York.
- HUIJUN, L., ZHICHAO, J., HUCHENG, Z., XIAOBING, W., JIANJI, W., 2018. *Photocatalysis oxidation activity regulation of Ag/TiO₂ composites evaluated by the selective oxidation of Rhodamine B*. App. Sur. Sci. 422, 1–10.
- HUNAG, Y.B., SHEN, M., WANG, X., HUANG, P., CHEN, R., LIN, Z.J., CAO, R., 2016b. *Water-medium C-H activation over a hydrophobic perfluoroalkane-decorated metal-organic framework platform*. J. Catal. 333, 1–7.
- HUNAG, Y.B., SHEN, M., WANG, X., SHI, P.C., LI, H., CAO, R., 2015. *Hierarchically micro- and mesoporous metal-organic framework-supported alloy nanocrystals as bifunctional catalysts: toward cooperative catalysis*. J. Catal. 330, 452–457.
- IBHADON, A.O., FITZPATRICK, P., 2013. *Heterogeneous photocatalysis: recent advances and applications*. Catalysts 3, 189–218.
- JEBAKUMAR, I.E.T.N., ATCHUDAN, R., SETHURAMAN, M.G., LEE, Y.R., 2016. *Reductive degradation of carcinogenic azo dyes using anacardiumoccidentaletesta derived silver nanoparticles*. J. Photochem. Photobiol. B: Biol. 162, 604–610.
- JIANG, R., LI, B., FANG, C., WANG, J., 2014. *Metal/semiconductor hybrid nanostructures for plasmon-enhanced applications*. Adv. Mater. 26, 5274–5309.
- JINGXIANG, L., BEI, C., JIAGUO, Y., 2017. *Surface modification and enhanced photocatalytic CO₂ reduction performance of TiO₂: a review*. App. Sur. Sci. 392, 658–686

- JINGXIANG, L., SHUOQI, Q., DIFA, X., CHUANJIA, J., BEI, C., 2018. *Direct evidence and enhancement of surface plasmon resonance effect on Ag-loaded TiO₂ nanotube arrays for photocatalytic CO₂ reduction*. *App. Sur. Sci.* 434, 423-432.
- JUN, L., JIMMY, C.Y., 1998. *An investigation on photocatalytic activities of mixed TiO₂-rare earth oxides for the oxidation of acetone in air*. *J. Photochem. Photobiol. A: Chemistry* 116, 63-67.
- KOWALSKA, E., MAHANEY, O.P., ABE, R., OHTANI, B., 2010. *Visible-light-induced photocatalysis through surface plasmon excitation of gold on titania surfaces*. *Phys. Chem. Chem. Phys.* 12, 2344-2355.
- LAVANYA, T., SATHEESH, K., DUTTA, M., JAYA, N.V., FUKATA, N., 2014. *Superior photocatalytic performance of reduced graphene oxide wrapped electrospun anatase mesoporous TiO₂ nanofibers*. *J. Alloys. Compd.* 615, 643-650.
- LI, F., LI, Q., KIM, H., 2013. *Spray deposition of electrospun TiO₂ nanoparticles with self-cleaning and transparent properties onto glass*. *Appl. Surf. Sci.* 276, 390-396.
- LIANG, M.S., KHAW, C.C., LIU, C.C., CHIN, S.P., WANG, J., LI, H., 2013. *Synthesis and characterisation of thin-film TiO₂ dye-sensitised solar cell*. *Ceram. Int.* 39, 1519-1523.
- LIANG, Y., LIN, S., HU, J., LIU, L., MCEVOY, J.G., CUI, W., 2014. *Facile hydrothermal synthesis of nanocomposite Ag@AgCl/K₂Ti₄O₉ and photocatalytic degradation under visible light irradiation*. *J. Mol. Catal. A Chem.* 383-384, 231-238.
- LIANG, Y., WANG, H., LIU, L., CUI, W., 2015. *Facile synthesis of Ag@AgCl plasmonic photocatalyst and its photocatalytic degradation under visible light*. *Rare. Metal. Mater. Engin.* 44(5), 1088-1093.
- LIU, W., CHEN, D., YOO, S.H., CHO, S.O., 2013. *Hierarchical visible light-response Ag/AgCl@TiO₂ plasmonic photocatalysts for organic dye degradation*. *Nanotechnology.* 24, 405706-405712.
- MA, X.C., DAI, Y., YU, L., HUANG, B.B., 2016. *Energy transfer in plasmonic photocatalytic composites*. *Light: Science & Applications* 5, 16017.
- MOLINARI, R., PIRILLO, F., FALCO, M., LODDO, V., PALSIMANO, L., 2004. *Photocatalytic degradation of dyes by using a membrane reactor*. *Chem. Eng. Process.* 43, 1103-1104.
- MURUGAN, K., SUBASRI, R., RAO, T.N., GANDHI, A.S., MURTY, B.S., 2013. *Synthesis, characterization and demonstration of self-cleaning TiO₂ coatings on glass and glazed ceramic tiles*. *Prog. Org. Coat.* 76, 1756-1760.
- NAKATA, K., OCHIAI, T., MURAKAMIA, T., FUJISHIMA, A., 2012. *Photoenergy conversion with TiO₂ photocatalysis: New materials and recent applications*. *Electrochim. Acta.* 84, 103-111.
- PARIDA, K.M., SAHU, N., 2008. *Visible light induced photocatalytic activity of rare earth titania nanocomposite*. *J. Mol. Catal. A: Chem.* 287, 151-158.
- PHAM, M.H., DINH, C.T., VUONG, G.T., TA, N.D., DO, T.O., 2014. *Visible light induced hydrogen generation using a hollow photocatalyst with two cocatalysts separated on two surface sides*. *Phys. Chem. Chem. Phys.* 16, 5937-5941.
- QI, L., YU, J., LIU, G., WONG, P.K., 2014. *Synthesis and photocatalytic activity of plasmonic Ag@AgCl composite immobilized on titanate nanowire films*. *Catal. Today.* 224, 193-199.
- QINGHONG, Z., LIAN, G., JINGKUN, G., 2000. *Effects of calcination on the photocatalytic properties of nanosized TiO₂ powders prepared by TiCl₄ hydrolysis*. *Appl. Catal. B: Environ.* 26, 207-215.
- RUIRUI, L., ZHIJIANG, J., JING, W., JINJUN, Z., 2018. *Solvothermal synthesized Ag-decorated TiO₂/sepiolite composite with enhanced UV-vis and visible light photocatalytic activity*. *Micropor. Mesopor. Mater.* 266, 268-275.
- SANCHEZ, E., LOPEZ, T., GOMEZ, R., BOKHIMI, MORALES, A., NOVARO, O., 1996. *Synthesis and characterization of sol-gel Pt/TiO₂ catalyst*. *J. Solid. Stat. Chem.* 122, 309-314.
- SHAHMOTADI, B., MALEK, A., BYRAPPA, K., 2011. *Photocatalytic degradation of amaranth and brilliant blue FCF dyes using in situ modified tungsten doped TiO₂ hybrid nanoparticle*. *Catal. Sci. Technol.* 1, 1216-1223.
- SIMMONS, E.L., 1975. *Diffuse reflectance spectroscopy: a comparison of the theories*. *App. Opt.* 14, 1380-1386.
- SLIMEN, H., LACHHEB, H., QOURZAL, S., ASSABBANE, A., HOUAS, A., 2015. *The effect of calcination atmosphere on the structure and photoactivity of TiO₂ synthesized through an unconventional doping using activated carbon*. *J. Environ. Chem. Eng.* 3, 922-929.
- TAYADE, R.J., SUROLIYA, P.K., KULKARNI, R.G., JASRA, R.V., 2007. *Photocatalytic degradation of dyes and organic contaminants in water using nanocrystal-line anatase and rutile TiO₂*. *Sci. Techn. Adv. Mater.* 8, 455-462.
- TURKTEN, N.; CINAR, Z., 2017. *Photocatalytic decolorization of azo dyes on TiO₂: Prediction of mechanism via conceptual DFT*. *Catal. Today.* 287, 169-175.
- VARGAS, D.X.M., ROSA, J.R.D.L., ORTIZ, C.J.L., RAMIREZ, A.H., ESCAMILLA, G.A.F., GARCIA, C.D., 2015. *Photocatalytic degradation of trichloroethylene in a continuous annular reactor using Cu-doped TiO₂ catalysts by sol-gel synthesis*. *App. Cata. B: Environ.* 179, 249-261.

- WANG, D., LI, Y., PUMA, G.L., WANG, C., WANG, P., ZHANG, W., WANG, Q., 2013. *Ag/AgCl@helical chiral TiO₂ nanofibers as a visible-light driven plasmon photocatalyst*. Chem. Commun. 49, 10367-10369.
- WEN, J., LI, X., LI, H., MA, S., HE, K., XU, Y., FANG, Y., LIU, W., GAO, Q., 2015. *Enhanced visible-light H₂ evolution of gC₃H₄ photocatalysts via the synergetic effect of amorphous NiS and cheap metal-free carbon black nanoparticles as co-catalysts*. Appl. Surf. Sci. 358, 204-212.
- XUE, X., JI, W., MAO, Z., MAO, H., WANG, Y., WANG, X., RUAN, W., ZHAO, B., LOMBARDI, J.R., 2012. *Raman investigation of nanosized TiO₂: effect of crystallite size and quantum confinement*. J. Phys. Chem. C. 116, 8792-8797.
- YAO, X., LIU, X., 2014. *One-pot synthesis of Ag/AgCl@SiO₂ core-shell plasmonic photocatalyst in natural geothermal water for efficient photocatalysis under visible light*. J. Mol. Catal. A Chem. 393, 30-38.
- YIN, H., WANG, X., WANG, L., NIE, Q., ZHANG, Y., YUAN, Q., WU, W., 2016. *Ag/AgCl modified self-doped TiO₂ hollow sphere with enhanced visible light photocatalytic activity*. J. All. Comp. 657, 44-52.
- ZHOU, J., ZHANG, Y., ZHAO, X.S., RAY, A.K., 2006. *Photodegradation of benzoic acid over metal-doped TiO₂*. Indus. Engin. Chem. Res. 45, 3503-3511.